




Streamer self-focusing in an external longitudinal magnetic fieldA. Yu. Starikovskiy ^{1,*}, N. L. Aleksandrov ², and M. N. Shneider ¹¹*Princeton University, Princeton, New Jersey 08544, USA*²*Moscow Institute of Physics and Technology, Dolgoprudny 141700, Russia*

(Received 25 January 2021; revised 2 April 2021; accepted 6 May 2021; published 1 June 2021)

The numerical simulation of the development of a streamer discharge in a gap with an external longitudinal magnetic field was used to demonstrate the self-focusing of such discharges. Self-focusing is caused by a sharp deceleration of the radial ionization wave due to a change in the electron energy distribution function, a decrease in the average electron energy, the rate of gas ionization, and the electron mobility in crossed electric and magnetic fields as compared to the case of the discharge development without a magnetic field. The self-focusing effect of a streamer discharge in an external longitudinal magnetic field is observed for both positive and negative pulse polarities. The paper proposes an estimate of the critical value of the magnetic field, which makes it possible to control the development of pulsed high-voltage discharges at various gas pressures.

DOI: [10.1103/PhysRevE.103.063201](https://doi.org/10.1103/PhysRevE.103.063201)**I. INTRODUCTION**

Magnetohydrodynamic (MHD) generators might be able to extract significant levels of power from the flow [1] to enable a direct electric power generation from a high-speed flow of combustion products and new high-power demand technologies including plasma steering, plasma-assisted drag reduction, combustion control, and suppression of shock-induced separation, all without the need for moving parts. The viability of MHD flow control and power extraction is expected to improve with increasing the flight altitude and velocity. The need to ionize a flow to make it conductive is perhaps the most significant challenge associated with MHD devices operating in Mach number regimes below about Mach 12 [2–4]. In this regime, even the viscous portions of the flow are cold enough such that seeding the flow with an alkali metal vapor will not lead to significant conductivity [2–4]. It has been shown that nonequilibrium ionization methods including electron beams or short, high-voltage pulses are the most efficient means of generating conductivity through the electron-impact gas ionization [2–6]. It has also been shown that by using a nonequilibrium ionization for MHD power extraction the amount of power that is coupled out of a hypersonic flow can be significantly higher than the theoretical power requirements for ionization [2–4]. Because of the large density gradients and resultant conductivity gradients associated with supersonic flows, volume-filling supersonic discharges are often difficult to produce in a wind tunnel.

In addition to MHD flow control and power generation, there are other applications that render such a discharge desirable. Carbon monoxide and excimer gas discharge lasers in general can benefit greatly from the use of a high throughput of cooled (in a supersonic nozzle) gas. To this end, supersonic discharges for pumping such lasers have been

reported in molecular flows using DC discharges [7–9], electron beam stabilization techniques [10], and a 13.56-MHz RF discharge [11]. Recent progress has been made at the Ohio State University also using a 13.56-MHz RF source to drive a volume-filling discharge in Mach 2.5 airflow [12]. Pulsed ionization schemes in conjunction with DC discharges have also been implemented successfully in subsonic flows to reduce arcing in CO₂ lasers. This has been demonstrated experimentally by Generalov *et al.* [13–15].

Electron-neutral collisions and their effect on the electrical conductivity strongly influence the nature of MHD interaction with the flow. The two most relevant parameters in assessing the effects of collisions in a nonthermally ionized MHD generator are the electron Hall parameter β_e and the electron loss rate. The Hall parameter is defined as the ratio of the electron gyrotron frequency $\omega_e = eB/m_e$ (B is a magnetic flux density, m_e is an electron mass, e is an elementary charge) to the electron transport collision frequency ν_e [16]. In air, the electron loss rate is dominated by attachment to oxygen at low temperatures and high gas densities and by dissociative electron-ion recombination at high ionization levels and lower gas densities [2–5]. The electron loss rate controls the energy required for nonthermal gas ionization.

Application of nanosecond high-voltage pulses to maintain uniform volumetric ionization in a supersonic flow is promising for use in MHD generators. Sustaining conductivity by high-voltage pulses has the great advantage of removing the requirement of the flow seeding and potentially extending the operability of MHD to lower temperatures and Mach numbers, since the conductivity is no longer directly related to thermal ionization of a low ionization potential material such as potassium. High-voltage pulses applied along the magnetic field lines play a dual role. First, a sufficiently high degree of ionization and uniformity of the generated plasma in the gas flow are maintained, and, second, the recombination decay of the plasma is significantly slowed down due to the periodic heating of electrons by the electric field of a high-voltage

*Corresponding author: astariko@princeton.edu

pulsed discharge. Such a scheme of an MHD generator supported by high-voltage pulses in a cold air flow was first implemented in 2006 at Princeton [17]. In this work, MHD power extraction using nonequilibrium ionization in a cold supersonic airflow has been observed. A volumetric, uniform, nonequilibrium cold plasma has been produced in a Mach 3 airflow using 2 ns, 100 kHz repetition rate, 30 kV pulses. Theoretical analysis indicated the electron number density to be on the order of $5 \times 10^{11} - 10^{12} \text{ cm}^{-3}$. The 5 T magnetic field was shown to improve the uniformity of the plasma and had a dramatic effect in confining the plasma to the interelectrode volume.

Thus, the development of nanosecond pulsed discharges in a strong external magnetic field is of significant interest both from the point of view of energy generation in the MHD cycle (for example, when burning natural coal in oxygen) and for the problems of possible CO₂ utilization using alternative renewable energy sources. However, for the successful operation of the MHD generator, the high efficiency of the homogeneous plasma production in the flow is required. When ionizing high-voltage pulses are applied, inhomogeneities can appear and develop during the pulse, creating thin plasma channels with a relatively high degree of ionization in the boundary layers and in the flow core. These inhomogeneities can lead to the development of instabilities in a weakly ionized plasma in crossed electric and magnetic fields (see, for example, [18,19]), which significantly reduce the efficiency of energy generation, or, in general, make the operation of the MHD generator impossible.

An example of a pulsed nanosecond discharge is a streamer characterized by fast-propagating ionization fronts with self-organized electric field enhancement at its tip. Streamer discharges have been much studied over many decades (see [20,21] and references therein). However, little is known about the effect of magnetic field on streamer properties and the number of works devoted to the development of pulsed discharges in strong magnetic fields is small. It was shown [22–25] that the application of a magnetic field can affect the evolution of an electron avalanche, the time of breakdown formation, and other breakdown characteristics. Moreover, a longitudinal magnetic field can suppress the development of the near-electrode instability in a non-self-sustained gas discharge [26,27]. It was experimentally observed that the streamer channels can be deflected under a transverse magnetic field when propagating in a free gas [28] and along a dielectric surface [29,30]. In all these studies, as a rule, the development of a discharge at high pressures and relatively weak magnetic fields was addressed, when the effect of a magnetic field was mainly reduced to a displacement of the discharge channel at long times. The propagation of a surface discharge at a relatively low (100 Torr) pressure and strong magnetic field ($B = 3 \text{ T}$) was studied only in the geometry in which the magnetic field was perpendicular to the electric field [29]. Here, the application of the magnetic field led to simply bending of the surface streamer trajectories. Surface discharges were also investigated at lower magnetic fields and higher pressures [30].

An attempt was made to develop an analytical model of a streamer in a longitudinal magnetic field, taking into account the change in the electron mobility across the magnetic field

lines [31]. In this study, the influence of the magnetic field on the average electron energy and electron impact ionization rate was not considered. Nevertheless, only taking into account the dependence of the electron mobility on the electric and magnetic field direction, the model led to the conclusion about a possible decrease in the radius of curvature of the streamer head and an increase in its propagation velocity when an external magnetic field is applied [31].

In the present work, a numerical characterization of nanosecond pulsed discharges has been conducted in a strong magnetic field environment. Streamer discharge development and plasma generation in pure CO₂ was analyzed when magnetic field was directed along the axis of the discharge cell. Numerical simulations were based on a two-dimensional fluid model. It was shown that a strong magnetic field affects dramatically the plasma formation. The nanosecond streamer diameter decreased significantly, whereas the plasma density increased with increasing the magnetic field amplitude. The mechanisms of the magnetic field interaction with the pulsed discharge development were discussed.

II. NUMERICAL MODEL OF NANOSECOND DISCHARGE DEVELOPMENT

To study the effect of a longitudinal magnetic field on streamer properties, we considered a solitary streamer developing in the 14 cm plane-to-plane discharge gap. A streamer was initiated near the high-voltage electrode and propagated to the ground plane electrode. The high-voltage electrode was a plate at $Z = 1 \text{ cm}$ with a semiellipsoidal needle (a major semiaxis of 0.8 cm and a minor semiaxis of 0.08 cm) protruded from the center of the plate (Fig. 1).

Calculations were made in an axisymmetrical geometry in Z - R coordinates. We used the spatial symmetry in the azimuth angle φ because the geometry of the discharge gap has the axial symmetry, which is not violated by the external magnetic field directed along the discharge gap axis. In this case, the 3D description is exactly reduced to the axially symmetrical 2D description when the discharge development is simulated in Z - R coordinates. The computational region was $15 \times 15 \text{ cm}^2$ (Fig. 1). The minimal grid size was $1.5 \mu\text{m}$, whereas the minimal time step was $5 \times 10^{-14} \text{ s}$. The adaptive grid changed with streamer development in the gap. The cell size increase was limited by 10% to avoid the numerical error increase on a nonuniform grid. The time step was determined according to the convergence condition by Courant-Friedrichs-Lewy and changed with changing electron drift velocity in a self-consistent electric field. The minimum space step and grid structure were the same in all cases under consideration (in magnetic field and in its absence) to avoid the effect of grid approximation on the calculated results. Numerical convergence in the calculations was tested for different grids.

Calculations were carried out for different magnetic field values at fixed gas pressure $P = 50 \text{ Torr}$, room gas temperature, and fixed nanosecond pulse voltage $U = 20 \text{ kV}$. We assumed that the applied voltage increased linearly to 20 kV for 1 ns and remained constant for $t > 1 \text{ ns}$.

Streamer initiation and propagation was simulated on the basis of an axially symmetric 2D fluid model [32–37]. The system of equations under study consisted of the transport

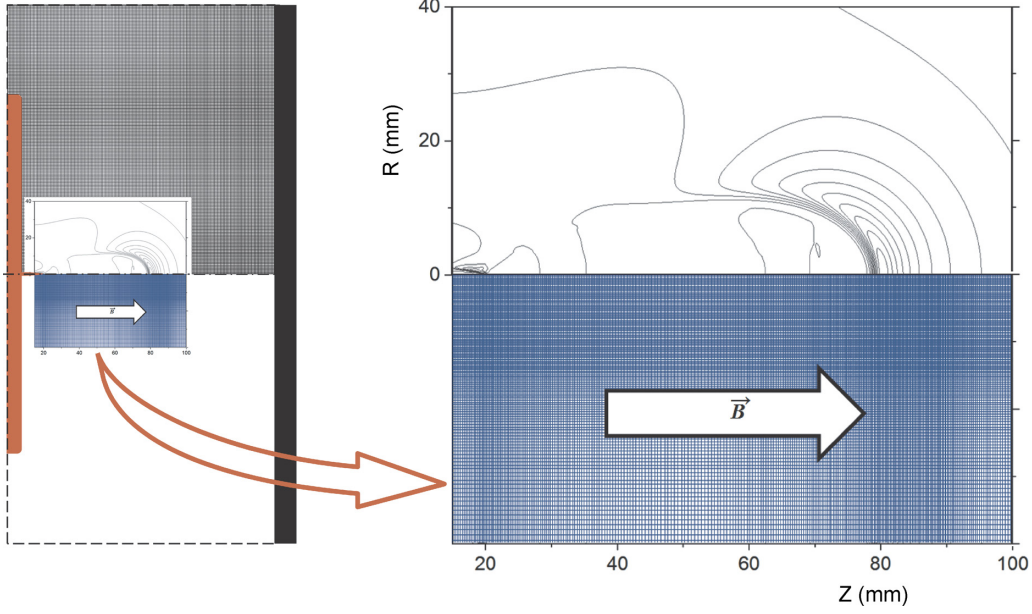


FIG. 1. Discharge gap geometry (left) and adaptive computational mesh (right). Left: The plane high-voltage electrode had a radius of $R = 100$ mm and was located at $Z = 8$ mm (marked by red). The tip of the high-voltage electrode needle was located at $Z = 20$ mm. The grounded plane electrode (black) was located at $Z = 150$ mm. The computational domain had a size of 150×150 mm² above Z axis (gray mesh). Right top: The contours of the electric field of the positive streamer 40 ns after the start of the high-voltage pulse. $P = 50$ Torr, $T = 293$ K, $U = +20$ kV, CO₂. Right bottom: The adaptive computational mesh (every 10th cell is shown).

equations for the densities of charged particles (electrons and positive and negative ions) and Poisson's equation for the electric field. The transport and kinetics of charged species were considered in the local approximation, whereas the nonlocal approach was utilized to describe photoionization generating seed electrons in front of the streamer head by ionizing radiation emitted from the head and the streamer channel:

$$\frac{\partial n_e}{\partial t} + \text{div}(\vec{u}_e \cdot n_e) = S_{\text{ion}} + S_{\text{photo}} - S_{\text{att}} - S_{\text{rec}}^{ei}, \quad (1)$$

$$\frac{\partial n_p}{\partial t} = S_{\text{ion}} + S_{\text{photo}} - S_{\text{rec}}^{ei} - S_{\text{rec}}^{ii}, \quad (2)$$

$$\frac{\partial n_n}{\partial t} = S_{\text{att}} - S_{\text{rec}}^{ii}, \quad (3)$$

$$\Delta\varphi = -\frac{e}{\epsilon_0}(n_p - n_e - n_n), \quad (4)$$

where S_{ion} is the ionization rate, S_{photo} is the rate of photoionization, S_{att} is the rate of electron attachment, and S_{rec}^{ei} and S_{rec}^{ii} are the rates of electron-ion and ion-ion recombination, respectively. n_p , n_n , and n_e are number density values for positive ions, negative ions, and electrons, φ is plasma potential, and ϵ_0 is a vacuum permittivity. Ionization of gas molecules by electron impact, electron attachment to molecules, and electron-ion and ion-ion recombination were taken into account. The photoionization term S_{photo} has been taken according to the data presented in [38].

The local electric field approximation for electrons is the classical approach in fluid models. More sophisticated methods such as extended (high-order) fluid models and hybrid models have been suggested to simulate streamer properties [21,39–43]. These methods in some cases are more adequate

for describing electron characteristics in gases under nonuniform electric field and electron density conditions. However, they are time consuming and difficult to use for simulating long streamers. Estimates of the nonlocal effects on the electron ionization rate in CO₂ under the conditions studied were made on the basis of the results obtained. The nonlocal correction to the ionization coefficient was estimated to be $\approx 1\%$ (see discussion below). Therefore, to simulate positive and negative streamers in a long (14 cm) CO₂ gap, we utilized the classical fluid model with the local electric field approximation allowing reasonable run time and memory consumption.

The magnetic field does not appear explicitly in Eqs. (1)–(4). Magnetic field affects the electron energy distribution function and hence the electron drift velocity \vec{u}_e and the rates of electron processes including the electron impact ionization rate S_{ion} and photoionization rate S_{photo} . The effect of magnetic field on electrons is anisotropic because the component of \vec{B} parallel to the electric field \vec{E} does not influence the electron properties, whereas the component of \vec{B} normal to the electric field \vec{E} has the most profound influence on the electrons. The influence of magnetic field on the electron characteristics is discussed in the next section.

III. MAGNETIC FIELD INFLUENCE ON EEDF

The electron impact ionization rate coefficient, the electron drift velocity u_e , and the effective electron temperature T_e were calculated by solving the Boltzmann kinetic equation in the two-term approximation using the BOLSIG+ code [44,45] and the self-consistent set of the electron cross sections in CO₂ [46]. The applicability of the two-term approximation for describing the electron energy distribution in a strong magnetic field is discussed in the Appendix. In this

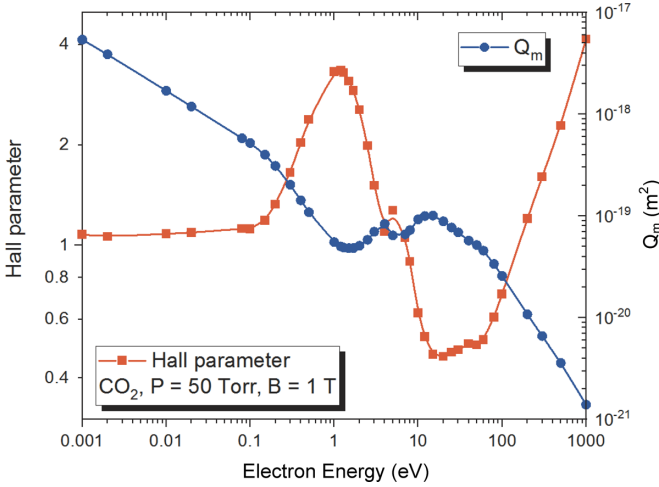


FIG. 2. Electron momentum cross section and Hall parameter versus electron energy for CO₂ at $P = 50$ Torr and $B = 1$ T.

approximation, the effect of magnetic field \vec{B} on the Boltzmann equation is reduced to the replacement of the electric field by the effective electric field E_{eff} [47],

$$E_{\text{eff}} = \sqrt{E_{\parallel}^2 + \frac{E_{\perp}^2}{[\beta_e(\varepsilon)]^2 + 1}}, \quad (5)$$

where E_{\parallel} and E_{\perp} are the longitudinal and transverse components of the electric field \vec{E} with respect to the magnetic field \vec{B} , respectively, $\beta_e(\varepsilon) = \omega_e/\nu_m(\varepsilon)$ is the Hall parameter for electrons with energy ε , $\nu_m(\varepsilon) = n \cdot u(\varepsilon) \cdot Q_m(\varepsilon)$ is the momentum transfer frequency for electrons with energy ε , $u(\varepsilon)$ is the electron velocity, $Q_m(\varepsilon)$ is the electron momentum cross section and n is the gas number density.

The electron energy distribution function is formed in weakly ionized plasma in a strong electric field by two processes. Electrons (i) gain energy from the electric field during their movement between collisions and (ii) lose energy in collisions with neutral particles. The application of a magnetic field deflects the electrons from their trajectories in the electric field and therefore hinders electron acceleration by the electric field. This happens only when the vector \vec{B} has a component normal to \vec{E} . If these vectors are parallel to each other, the magnetic field does not influence electron movement along the electric field. In this case, from (5), the effect of magnetic field on the electron energy distribution function (EEDF) is absent. This effect is most profound when the vector \vec{B} is perpendicular to the vector \vec{E} and $\beta_e \gg 1$. Here, the application of magnetic field inhibits drastically electron heating by the electric field and the effective electric field E_{eff} decreases.

Magnetic field affects equally all electrons when $Q_m(\varepsilon) \sim \varepsilon^{-0.5}$. Under such a condition the frequency $\nu_m(\varepsilon)$ and the Hall parameter are independent of ε . Figure 2 shows the electron momentum transfer cross section Q_m for CO₂ and the corresponding Hall parameter versus the electron energy for $P = 50$ Torr, room gas temperature, and $B = 1$ T. Because of a complicated energy dependence of $Q_m(\varepsilon)$ in CO₂, the effect of magnetic field is most profound for the electrons with energies between 0.1 and 4 eV and is the smallest for the electrons with

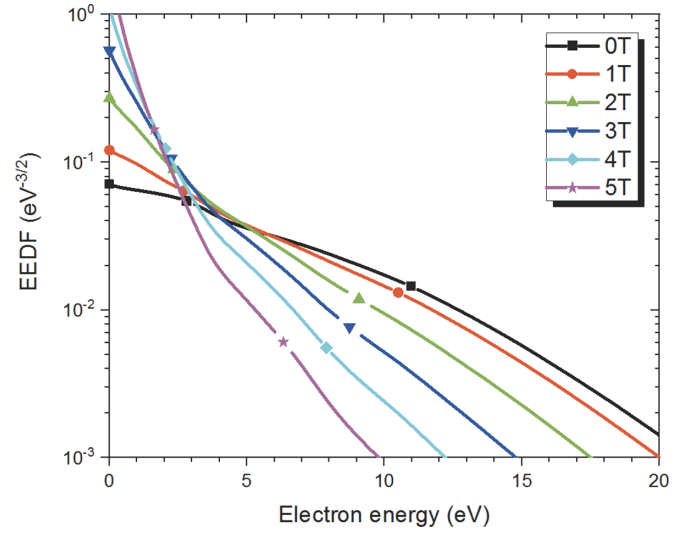


FIG. 3. Electron energy distribution functions in CO₂ for $E/n = 300$ Td, $P = 50$ Torr, and various values of magnetic field. The electric and magnetic fields are perpendicular to each other.

energies in the range 4–150 eV. As a result, the shape of the EEDF changes under the action of magnetic field. Figure 3 shows the calculated EEDF in CO₂ for $E/n = 300$ Td, 50 Torr, room gas temperature, and various values of magnetic field when it is perpendicular to the electric field. (Here, n is the gas number density; $E/n = 1$ Td = 10^{-17} V cm² corresponds to $E = 25$ kV/m for $P = 1$ atm and $T = 293$ K.) From this figure, the slopes of the curves at sufficiently high B are more gradual for $\varepsilon > 4$ eV in comparison with the slopes for lower electron energies. The shape of EEDF influences the electron transport and ionization rate coefficients, which control a streamer development in crossed electric and magnetic fields.

In a general case, the electron properties depend not only on the values of electric and magnetic fields, but on the angle α between these vectors as well. To take into account all possible combinations of \vec{B} and \vec{E} , we generated a lookup table over B , E , and $\cos(\alpha)$ values, and then constructed analytical functions to interpolate the rate and mobility coefficients in the entire range of the parameters B , E , and $\cos(\alpha)$. This approach dramatically reduced the computation time.

Figure 4 shows the result of the combined effect of electric and magnetic fields on the electron ensemble characteristics. EEDF and electron properties are not affected by magnetic field if the magnetic field vector \vec{B} is collinear to the electric field vector \vec{E} [$\cos(\alpha) = 1$]. When the electric field vector is perpendicular to the magnetic field vector [$\cos(\alpha) = 0$], the influence of the magnetic field becomes very strong and increases with the decrease of the electric field value. Figure 4(a) demonstrates the effect of an external magnetic field on the average electron energy in the case of perpendicular electric and magnetic fields [$\cos(\alpha) = 0$]. In the absence of magnetic field, the average electron energy $\langle \varepsilon \rangle$ begins to grow rapidly at $E/n > 10$ Td and reaches 1 eV already at $E/n \sim 31$ Td. An increase in the magnetic field leads to a decrease in $\langle \varepsilon \rangle$. The electric field required to obtain $\langle \varepsilon \rangle = 1$ eV is $E/n \sim 58$ Td for $B = 1$ T, 147 Td for $B = 3$ T, and 960 Td for $B = 20$ T.

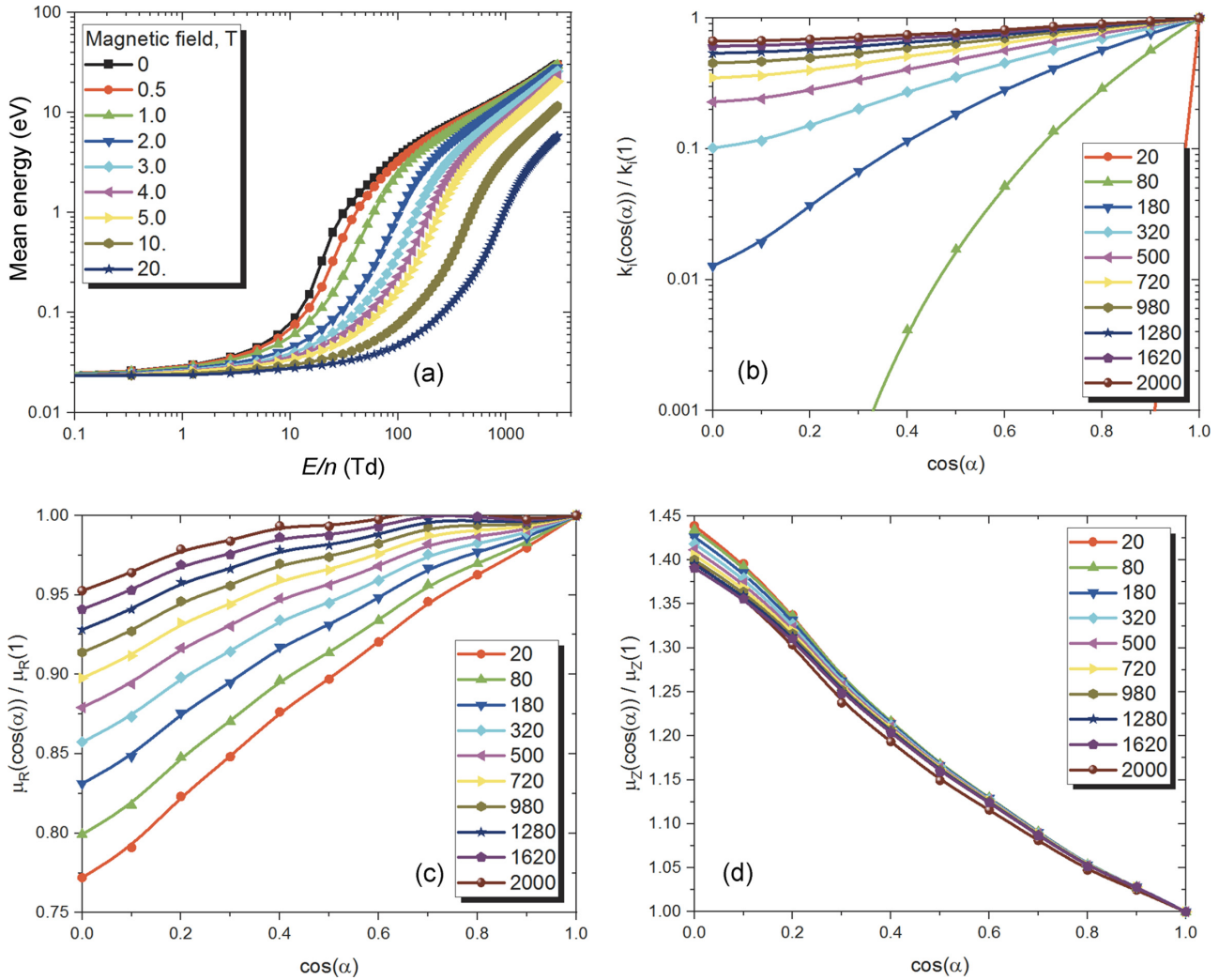


FIG. 4. (a) Mean electron energy versus E/n for $\cos(\alpha) = 0$ and different B . (b)–(d) Ionization rate coefficient k_i and electron mobility along the magnetic field vector (μ_Z) and across the magnetic field vector (μ_R) versus $\cos(\alpha)$ for $B = 3$ T and different E/n (scales in Td).

Such a strong dependence of the average electron energy on the magnitude of the perpendicular magnetic field obviously leads to a strong decrease in the rate of gas ionization by electron impact in an ionization wave propagating across the magnetic field lines. At the same time, the same magnetic field directed along the electric field vector does not cause any change in the ionization rate [Fig. 4(b)]. It can be seen that the decrease in the ionization rate in a radial ionization wave (propagating across the magnetic field lines) compared to a longitudinal wave (propagating along the magnetic field lines) is two orders of magnitude at $E/n = 180$ Td, and one order of magnitude at $E/n = 320$ Td. Even in a very strong electric field ($E/n \sim 1000$ Td), a twofold decrease in the ionization rate in the radial wave compared to the longitudinal wave is observed for a relatively weak magnetic field of $B = 3$ T. The effect is enhanced with the magnetic field increase and weakens with increasing E/n [Fig. 4(b)].

Another consequence of the appearance of a strong magnetic field directed along the streamer axis is a sharp decrease in the electron mobility in the radial (across the magnetic field lines) direction [Fig. 4(c)]. As in the case of the

ionization coefficient, the greatest decrease in the mobility is obtained in weak electric fields. At high E/n , the effect of the transverse magnetic field on the electron drift in the radial direction weakens. At the same time, the electron mobility in the direction of the magnetic field only slightly depends on the magnitude of the electric field and strongly depends on the direction of the magnetic field relative to the electric one [Fig. 4(d)]. Such a strong influence of the magnetic field on the electron ensemble characteristics, of course, should affect the development of discharges in the gas. In the next section, we will consider this effect for a streamer discharge.

IV. STREAMER PROPAGATION DYNAMICS IN STRONG EXTERNAL MAGNETIC FIELD

We made a numerical modeling of the development of a nanosecond streamer discharge in a strong external magnetic field directed along the axis of the discharge gap.

The calculations were carried out for CO_2 pressure of $P = 50$ Torr, room gas temperature, and a voltage of

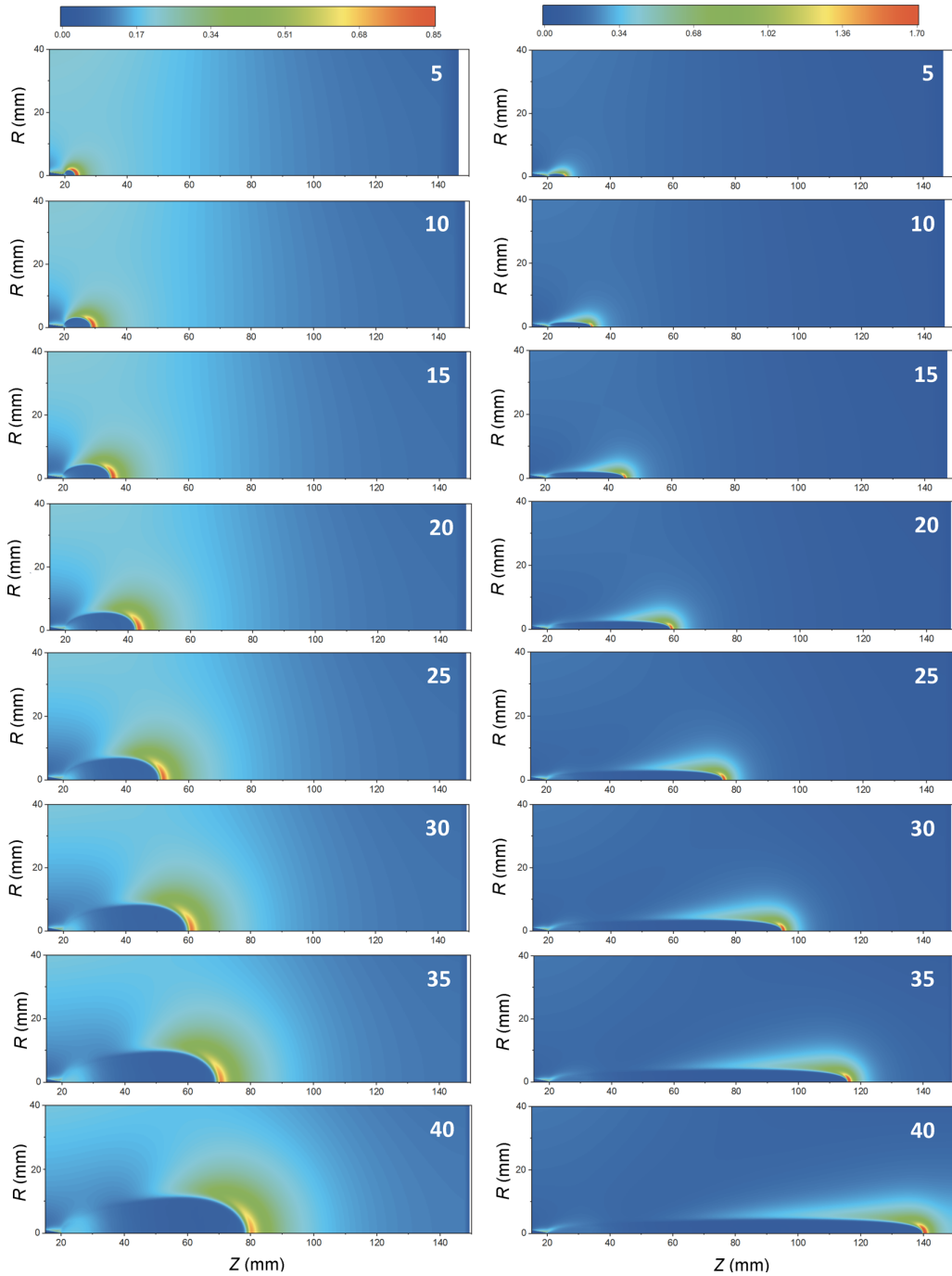


FIG. 5. Spatial electric field distribution during the development of a positive streamer for $B = 0$ (left) and $B = 3$ T (right). Left scale: 0–0.85 MV/m. Right scale: 0–1.7 MV/m. $P = 50$ Torr, CO_2 , $U = +20$ kV. Numbers are time in nanoseconds.

$U = 20$ kV across the gap. The magnitude of the magnetic field was varied from 0 to 20 T, which corresponds to the reduced gyrofrequency

$$\omega_e/n = \frac{eB}{m_e n} = 0\text{--}20 \times 10^{-13} \text{ rad} \times \text{m}^3/\text{s}.$$

Figure 5 shows the dynamics of the spatial electric field distribution during the development of a positive streamer for $B = 0$ (left) and $B = 3$ T (right). From the figure, the radial ionization wave development is significantly suppressed in

the presence of the magnetic field due to inhibiting electron heating in the electric field when these fields are perpendicular to each other. As a result, the streamer diameter sharply decreases, whereas its propagation velocity grows. The electric field at the streamer head almost doubles.

This behavior of the streamer discharge in the longitudinal magnetic field can be interpreted as a self-focusing effect, because the discharge modified the gas medium such that the streamer diameter gradually decreased during the discharge propagation.

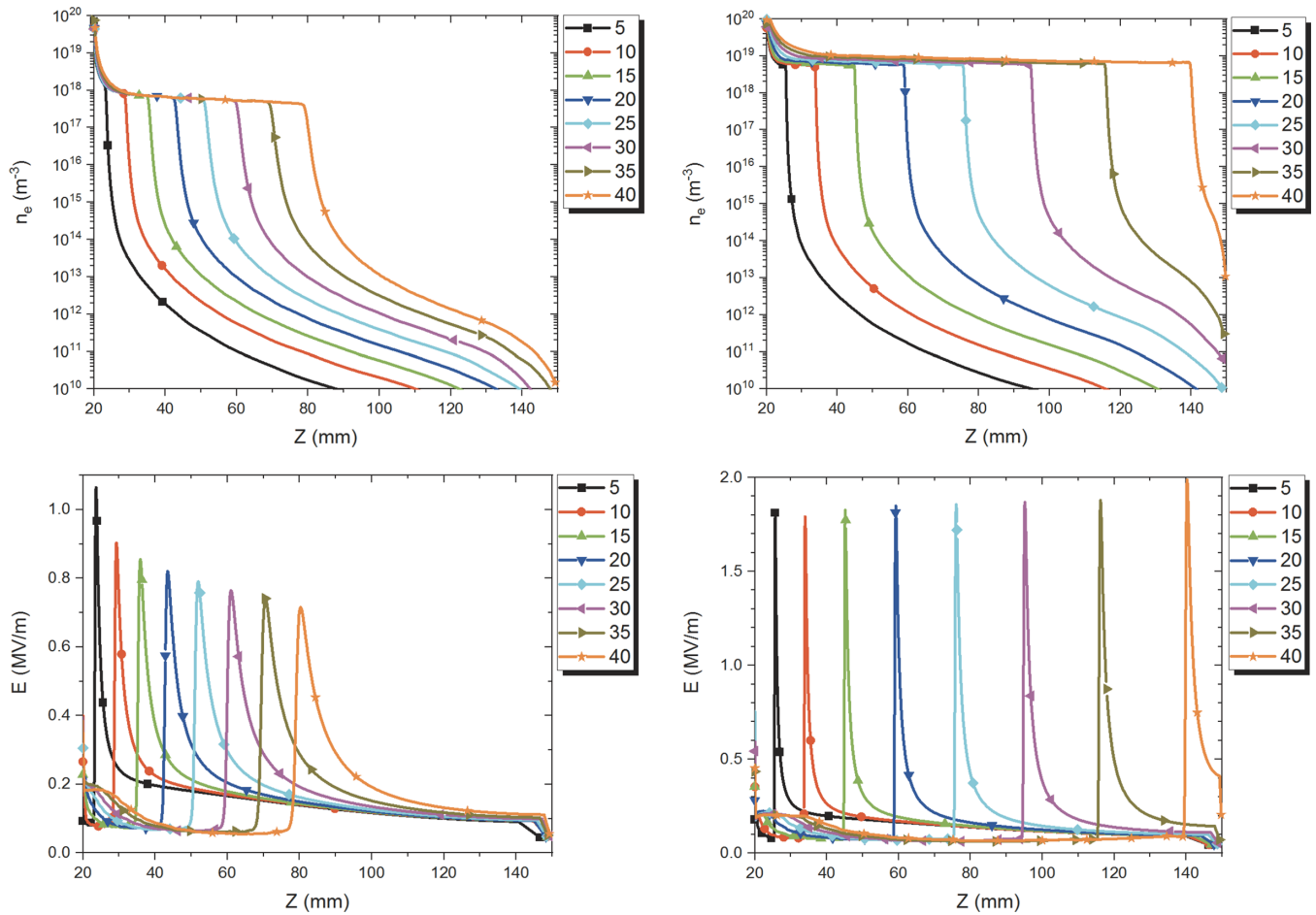


FIG. 6. Temporal evolution of the axial profiles of the electron density (upper row) and electric field (bottom row) during positive streamer development for $B = 0$ (left) and $B = 3$ T (right). Calculations are for $P = 50$ Torr, CO_2 , and $U = +20$ kV. The legend shows time from the discharge start in nanoseconds.

Figure 6 shows the temporal evolution of the axial profiles of the electron density and electric field during the positive streamer development in a magnetic field and in its absence. The streamer developing in the strong magnetic field has an almost an order of magnitude higher electron density in the channel (upper row), a higher electric field on the head, and much slower attenuation as it moves through the gap. At the same time, the electric field in the streamer channel remains almost the same in both cases. The electric field in the streamer channel is $E = 0.56$ kV/cm at $B = 0$ and $E = 0.62$ kV/cm at $B = 3$ T. An increase in the electron density in the channel and an increase in the plasma conductivity with the streamer development in the magnetic field leads to a decrease in the electric field in the channel. However, this electric field decrease is compensated by the electric field enhancement due to an increase in the streamer speed and a decrease in the channel diameter. As a result, the magnitude of the electric field in the streamer channel is almost the same with the magnetic field and without it (Fig. 6).

Figure 7 compares the channel radius, propagation velocity, and discharge current for a positive streamer propagating at $B = 0$ and $B = 3$ T. The radius of the streamer channel propagating without magnetic field is 2.5 times that of the streamer channel in the magnetic field. The opposite relation

is observed for the propagation velocity. The streamer in the magnetic field propagates 3 times faster than the streamer at $B = 0$. As a result, the streamer current in the magnetic field is double that without magnetic field (Fig. 7).

As mentioned above, an important parameter that determines the interaction of an electron ensemble with a magnetic field is the Hall parameter $\beta(\langle \varepsilon \rangle) = \omega_e / \nu_e$, which is the ratio of the gyrotron frequency of electrons in a magnetic field to the total frequency of electron transport collisions. As a rule, the effect of magnetic field becomes significant if the Hall parameter is higher than unity. Figure 8 shows the spatial distribution of the Hall parameter $\beta(\langle \varepsilon \rangle)$ and the average electron energy $\langle \varepsilon \rangle$ when the streamer is moving in the gap with a magnetic field of $B = 3$ T. From this figure, the Hall parameter is relatively small at the streamer head where the magnetic field vector is parallel to the vector of the electric field, while the average electron energy and the electron transport frequency are high. As a result, here, we have $\beta(\langle \varepsilon \rangle) = 1.5-1.7$ (Fig. 8).

Different values of the parameters under consideration are obtained on the lateral surface of the streamer channel. Here, the vector of the local electric field is perpendicular to the vector of the magnetic field. The electron energy and the ionization rate sharply decrease (Fig. 8) and the Hall

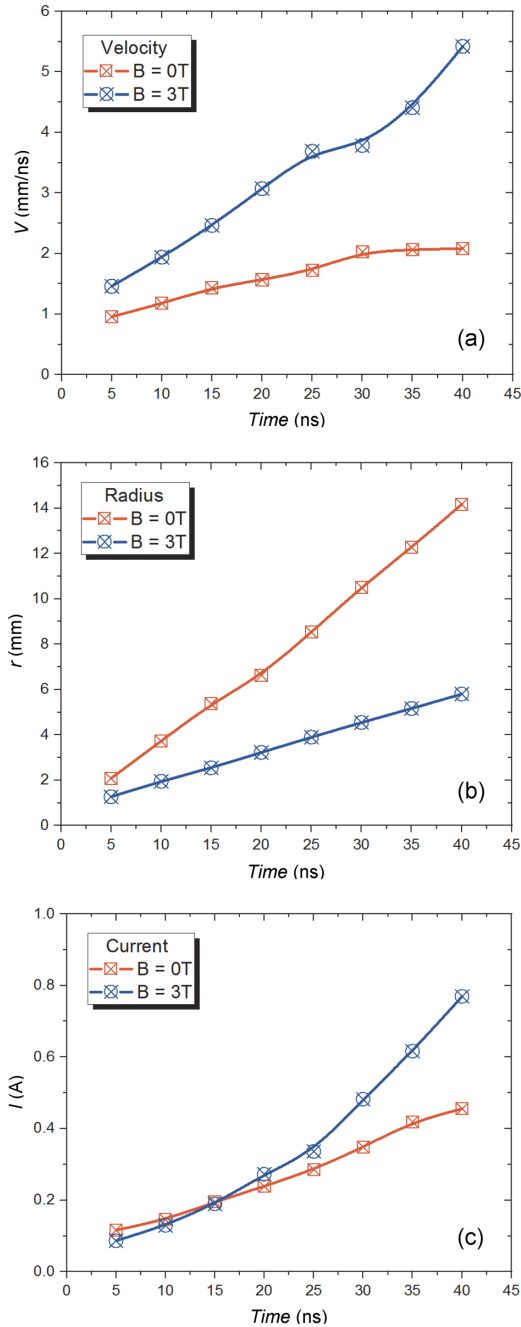


FIG. 7. Temporal evolution of the propagation velocity (a), channel radius (b), and discharge current (c) for a positive streamer propagating CO_2 . $P = 50$ Torr, $U = +20$ kV.

parameter becomes twice as large as that at the leading ionization wave. Thus, the Hall parameter increases from 1.5 at the streamer head to 3 on the lateral surface of the channel. This increase leading to a decrease in the ionization rate, as well as a low transverse electron mobility, clearly shows the mechanism of suppression of the radial ionization wave development during the streamer discharge propagation along a strong magnetic field in the discharge gap.

In the first 20 nanoseconds after the start, the streamer traveled 40 mm; that is, its average speed was 2 mm/ns (Fig. 8).

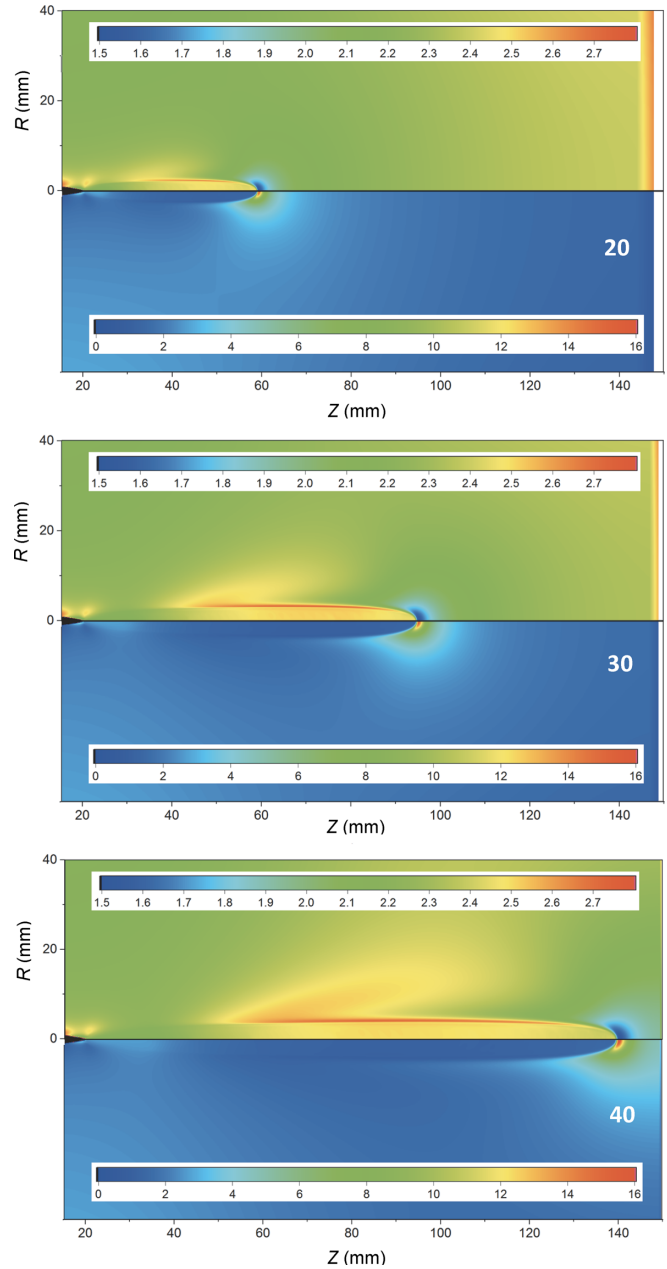


FIG. 8. Temporal evolutions of the spatial distributions of the Hall parameter (upper part of the image) and electron mean energy (lower part of the image) for a positive streamer developing in a magnetic field of $B = 3$ T. Scale for Hall parameter: 1.5–2.8. Scale for $\langle \epsilon \rangle$: 0–16 eV. $P = 50$ Torr, CO_2 , $U = +20$ kV. Numbers are time in nanoseconds.

In this case, the average electron energy was 16 eV in the head on the streamer axis and 3 eV at the radial ionization wave on the lateral surface of the channel. Over the next 10 ns, the streamer traveled another 35 mm. Here, the average streamer speed increased to 3.5 mm/ns due to a reduction in the radius of the curvature of the leading ionization wave front and an increase in the average field in the gap. The ratio of the Hall parameter on the streamer head and that on the streamer lateral surface remained practically the same as in the previous interval. A pronounced side lobe of high values

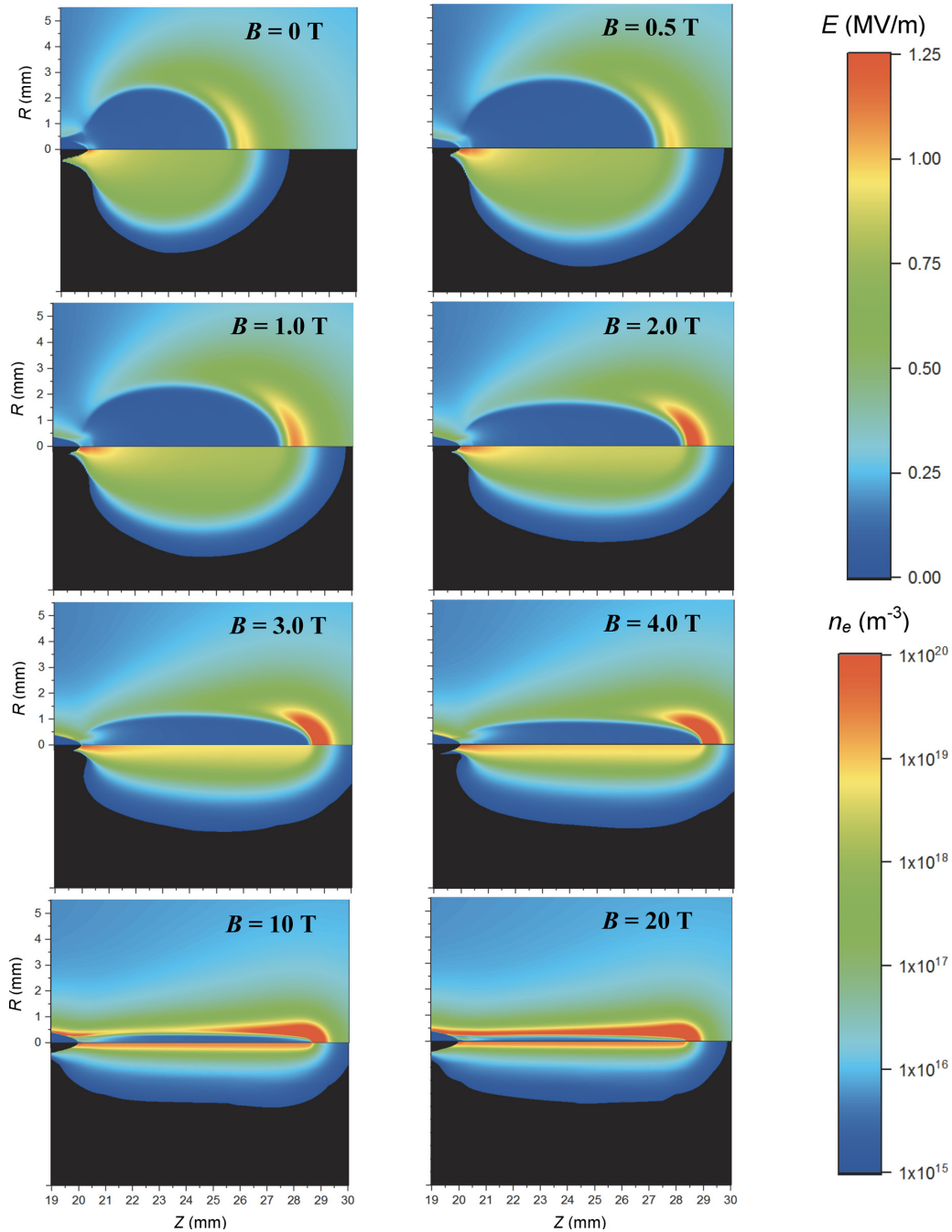


FIG. 9. Spatial distributions of the electric field (upper part of the image) and electron density (lower part of the image) for the positive streamer propagation in different magnetic fields. $P = 50$ Torr, CO_2 , $t = 7.0$ ns after high-voltage pulse start, $U = +20$ kV.

of the Hall parameter appeared near $Z = 50$ mm, which was associated with the spatial structure of the electric field in the discharge gap and a local decrease in the average electron energy far from the high-voltage electrode and the streamer head. The same distribution of the discharge parameters is preserved for $t = 40$ ns (Fig. 8). The streamer velocity in the gap increased to 4.5 mm/ns due to the electric field enhancement when approaching the grounded electrode. The Hall parameter remained high [$\beta(\langle \varepsilon \rangle) \sim 3$] on the lateral surface of the streamer and approximately 50% lower on its head. Thus, the interaction of electrons with a magnetic field leads to a significant decrease in the average electron energy in the

radial ionization wave, which prevents the streamer channel from expanding.

V. INFLUENCE OF DISCHARGE POLARITY

Figure 9, $B = 0$, demonstrates the initial phase of the positive streamer development near the tip of the high-voltage electrode in the absence of magnetic field. At a voltage rise rate of 20 kV/ns, the streamer does not have time to noticeably increase the radius until the instant when the voltage reaches its maximum value. The electric field at the leading

ionization wave becomes high and practically independent of direction.

In the absence of magnetic field, this means a high average electron energy and a high ionization rate in the ionization wave for all directions of its propagation. As a result, the channel rapidly expands and the electric field at the streamer head decreases to a typical value of $E \sim 1$ MV/m, which corresponds to the reduced electric field $E/n \sim 600$ Td at $P = 50$ Torr.

In the case of a longitudinal magnetic field in the discharge gap, the local electric field on the lateral streamer surface is perpendicular to the magnetic field. Here, the average electron energy and the electron impact ionization rate are significantly reduced due to the interaction of the electron ensemble with the magnetic field. Under such conditions, the radial ionization wave is significantly suppressed. Its speed decreases and the streamer radius remains much smaller compared to that in the absence of the magnetic field. A decrease in the radius of the streamer head leads to an increase in the electric field on it, and an increase in the velocity of the longitudinal ionization wave. As a result, the streamer becomes thinner with an increase in the longitudinal magnetic field in the gap, and its speed increases with B (Fig. 9).

Figure 10 shows the development of a negative streamer at different magnetic fields in the gap. The negative streamer propagates faster than the positive streamer because of the low efficiency of photoionization, which controls the positive streamer propagation, at low gas pressure. Therefore, Fig. 10 presents the spatial distributions of the electric field and electron density at $t = 4.2$ ns after the start of the discharge rather than at $t = 7.0$ ns, as in the case of the positive streamer.

The general behavior of the negative streamer is similar to that of the positive streamer. When the magnetic field exceeds 1 T, the characteristics of the negative streamer change due to the effect of the magnetic field on the EEDF and integrated electron coefficients.

As in the case of the positive streamer, when the magnetic field increases in the gap, the radius of the streamer channel sharply decreases, whereas the electric field on the streamer head, the propagation velocity, and the electron density in the channel increase (Fig. 10).

However, there is an important difference between the propagation of negative streamers and positive ones. Strong negative streamers, as well as strong positive streamers, propagate due to photoionization of the gas ahead of the wave front and electron impact ionization in the high electric field at the streamer head [48]. In addition, negative streamers have the mechanism of propagation in the “weak” regime due to the forward electron drift, which is absent in the case of positive polarity [48].

This difference in the propagation mechanisms becomes especially important when the propagation distance of the photoionizing radiation becomes much larger than the characteristic radius of the streamer channel [48,49]. This leads to a decrease in the efficiency of photoionization and significantly slows down the propagation of positive streamers. This effect should be especially pronounced at the highest values of the magnetic field, when the head radius of the propagating streamer is minimal.

Comparison of the streamer velocities calculated for positive and negative polarities of the high-voltage pulse clearly shows these different trends. The velocity of the negative streamer continuously increases as the magnetic field in the gap increases (Fig. 10). The positive streamer sharply accelerates with an increase in the magnetic field for $B < 4$ T and slows down with increasing B at $B > 4$ T. This deceleration is explained by a decrease in the efficiency of photoionization at small radii of the positive streamer head [48,49].

The difference between the behavior of the positive streamer and negative one is more pronounced in Fig. 11, which shows the axial profile of the electron density and electric field for different discharge polarities and magnetic fields. The negative and positive streamers behave almost identically when the magnetic field increases from 0 to 4 T. Here, the streamer speed, the electric field on the head, and the electron density increase with B . A further increase in the magnetic field leads to opposite results for the streamers of different polarities. The positive streamer slows down with further increase in B .

On the contrary, the negative streamer accelerates sharply and the electron density in the streamer channel increases with further increase of the magnetic fields. This is due to the positive feedback arising from the suppression of the radial ionization wave. In the strong magnetic field, the electrons can drift only forward along the axis of the discharge.

Such a displacement of the negative charge along the axis leads to an increase in the local axial electric field (Fig. 11, bottom row) and favors the electron impact ionization on the discharge axis where the magnetic field is parallel to the electric field and does not reduce the ionization rate. The strong ionization leads to an increase in the electron density and an increase in the rate of charge transfer along the axis. Self-focusing of the streamer is observed, which causes a decrease in the effective radius of the streamer head and an increase in the local electric field in its vicinity.

For the positive streamer, such a self-focusing is limited by the mean-free path of UV photons and nonlocal gas preionization in front of the streamer. Thus, the direction of the electron drift in the streamer head determines the different behavior of the positive and negative streamers at the high magnetic fields (Fig. 11). This conclusion has been made in [48,49] for the streamer propagation in the discharge gap without magnetic field. The present results extend the conclusion made in [48,49] to the case of strong external magnetic fields.

Figure 12 summarizes the data on the influence of the magnetic field on the radius of the streamer channel, discharge current, and the velocity of streamer propagation. The magnetic field increase from 0 to 4 T leads to a decrease in the streamer radius almost by an order of magnitude. Here, the streamer propagation velocity increases monotonically. As the magnetic field increases from 0 to 4 T, the ionization wave propagation velocity almost doubles due to a decrease in the radius of the conducting channel and an increase in the local field at the streamer head (Fig. 10). Figure 12 shows that the radial ionization wave weakens and the streamer radius decreases with increasing magnetic field because of the suppression of the radial electrons drift and significant decrease of the mean electron energy on the lateral streamer surface.

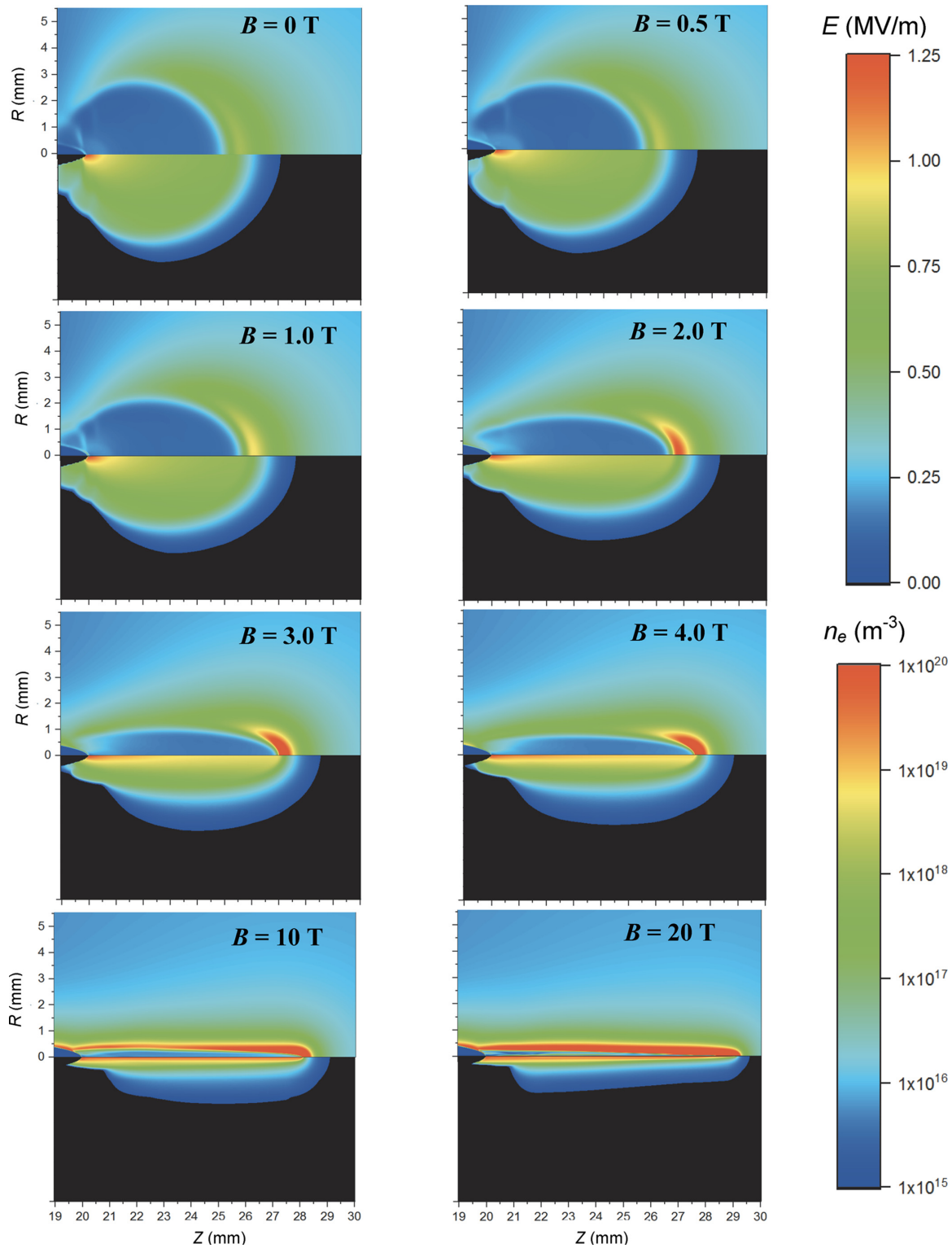


FIG. 10. Spatial distributions of the electric field (upper part of the image) and electron density (lower part of the image) for the negative streamer propagation in different magnetic fields. $P = 50$ Torr, CO_2 , $t = 4.2$ ns after high-voltage pulse start, $U = -20$ kV.

On the basis of the results obtained, it is possible to estimate the nonlocal effects on the electron transport and rate coefficients used in our simulation of the streamer properties in a magnetic field. The nonlocal effects on the rates of electron-molecule reactions are more profound than the effects on the electron transport coefficients [50]. Therefore, we

considered the electron ionization coefficient at the streamer head in CO_2 taking into account the nonuniformity (in space and time) of E/n and n_e . In the theory of perturbation, the space-dependent rate coefficient is represented as a sum of the local value and the product of the coefficients α_i dependent on the local field and the gradients of E/n and n_e [51]. Taking

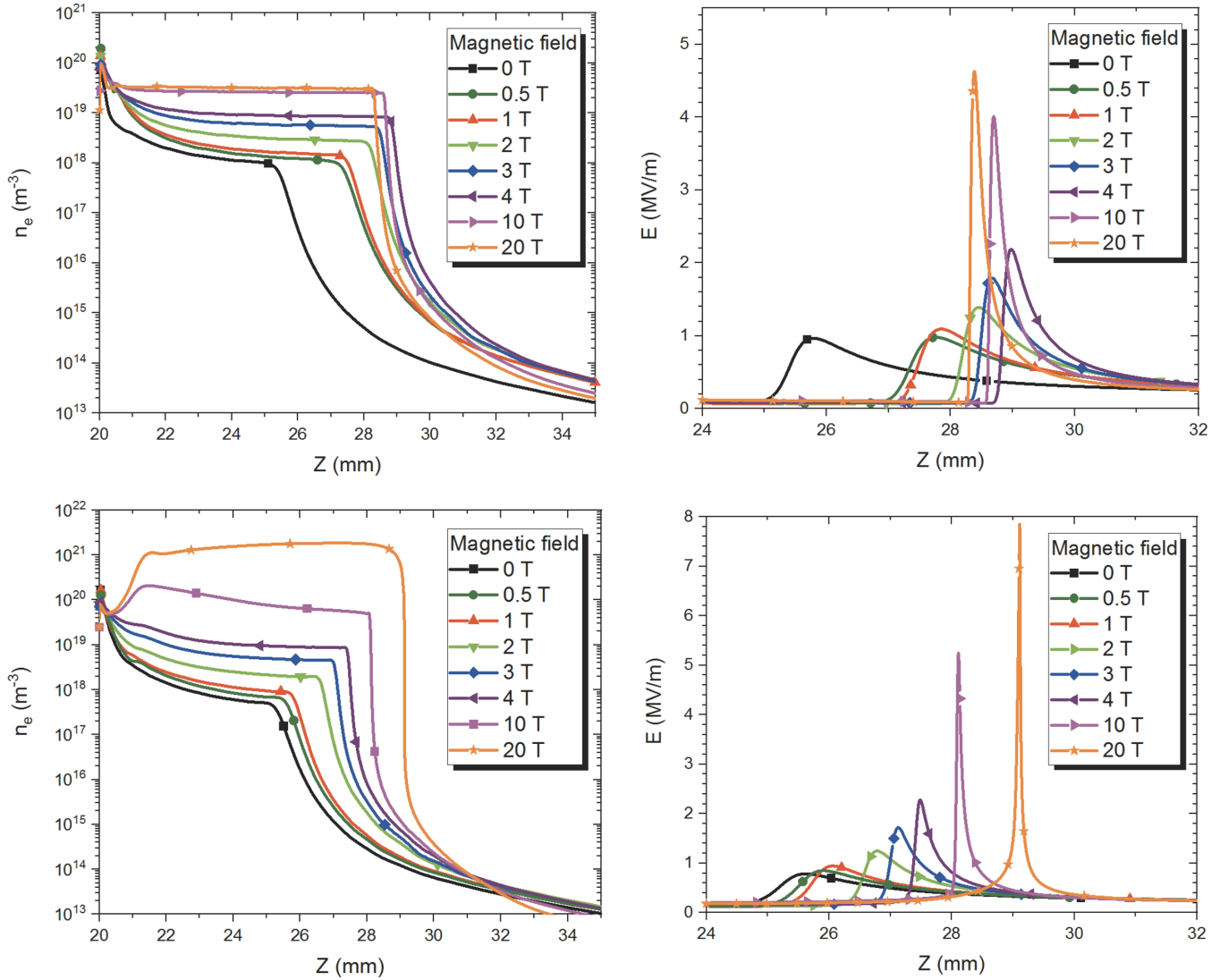


FIG. 11. Axial profiles of the electron density and electric field for different discharge polarities and magnetic fields. Top: Positive polarity, $t = 7.0$ ns. Bottom: Negative polarity, $t = 4.2$ ns. $P = 50$ Torr, CO_2 , $U = 20$ kV.

$B = 3$ T, $E = 1$ MV/m (see Figs. 6 and 12), the estimated correction to the electron ionization coefficient was $\approx 1\%$. Here, we used the calculated coefficients κ_i for CO_2 , whereas the gradients of E/n and n_e were estimated assuming that the spatial scale for variation of E/n and n_e is ≈ 0.1 cm (see Fig. 12). From Fig. 12, this scale decreases by a factor of five when B increases from 3 to 20 T. However, in this case, the values of κ_i decrease in a similar way. As a result, the estimated nonlocal effect on the ionization coefficient turns out to be almost independent of B and small in comparison with unity. In addition, we obtained similar estimated results for the unsteady effect (the influence of the variation in time of E/n) on the electron ionization coefficient using the calculated data for the perturbation theory in CO_2 for a time-varying electric field [52]. The temporal scale for variation of E/n was estimated to be the spatial scale for electric field variation divided by the streamer velocity. It may be concluded that the local electric field approximation for the electron energy distribution function and rate coefficients is acceptable when

simulating streamers in long CO_2 gaps under the conditions studied.

VI. CRITICAL MAGNETIC FIELD

It may be concluded that the streamer discharge sharply changes its characteristics with increasing the magnetic field from 0 to 4 T. With further increase in the magnetic field, the discharge parameters change much more smoothly. Thus, the reduced electron gyrofrequency $\omega_e/n \sim 10^{-13}$ rad \times m³/s corresponding to $B = 4$ T at 50 Torr is an important threshold above which the radial expansion of a streamer discharge in CO_2 is significantly suppressed. It should be noted that the reduced electron gyrofrequency is not a universal criterion for determining the threshold magnetic field, which allows one to significantly control the development of a pulsed high-voltage discharge. This value could change significantly due to different electron momentum transfer cross sections $Q_m(\varepsilon)$ in gases and different dependencies of the average electron

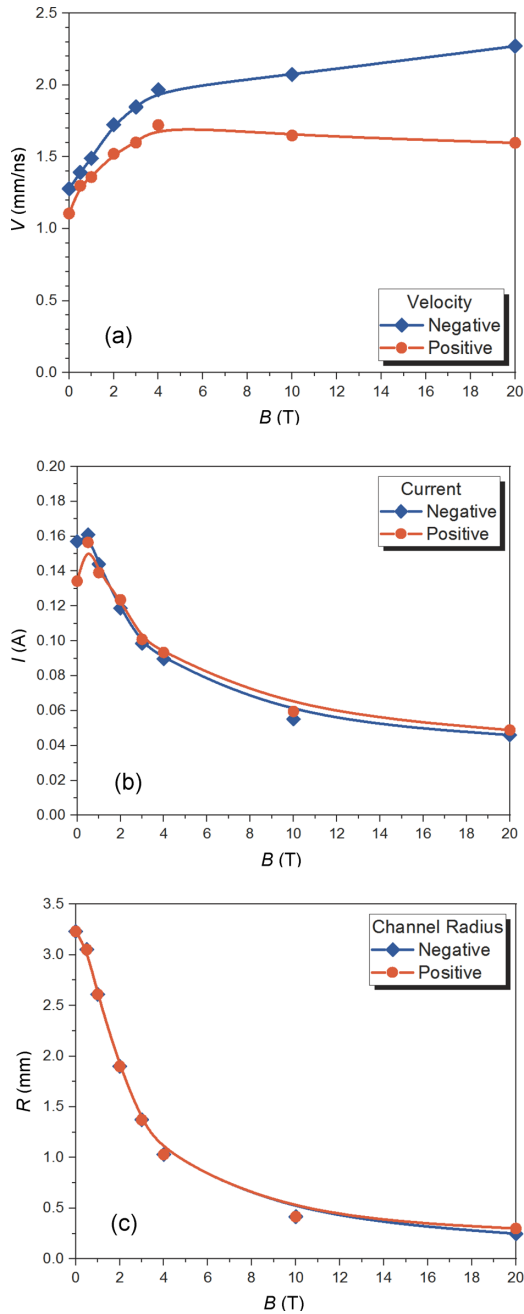


FIG. 12. Streamer velocity (a), discharge current (b), and channel radius (c) versus magnetic field for different voltage polarities. Positive polarity, $t = 7.0$ ns. Negative polarity, $t = 4.2$ ns. $P = 50$ Torr, CO_2 , $U = 20$ kV.

energy on E/n . The most appropriate criterion should be based on the Hall parameter, which is the ratio of the electron gyrofrequency to the electron momentum transfer frequency ν_e . As noted above, the effect of the magnetic field is significant when the Hall parameter exceeds unity. However, to calculate the value of the Hall parameter, it is required to know the distribution of the electric field in the discharge gap (Figs. 3 and 8). Generally speaking, a complete calculation of the discharge development in the magnetic field should be made. At the same time, the reduced electron gyrofrequency ω_e/n depends only on the initial parameters of the problem

and could be a convenient estimate of the possible influence of external magnetic field on the discharge development, by analogy with the reduced electric field E/n in the gap.

By extrapolating the values obtained in this work to normal conditions (atmospheric pressure and room gas temperature), it can be estimated that a longitudinal magnetic field significantly affects the development of a high-voltage discharge only at $B > 15$ T and that the magnetic field controls the development of such a discharge at high pressure for $B > 60$ T. These considerations limit the area of application of such methods to relatively low gas densities or ultrasmall discharge gaps with strong magnetic fields. At the same time, for pressures up to 100 Torr, even relatively low magnetic fields in the gap can dramatically change the characteristics of a pulsed discharge development, causing strong discharge self-focusing.

VII. CONCLUSIONS

Thus, based on the results of numerical simulation of the development of a streamer discharge in CO_2 in a gap with an external longitudinal magnetic field, the possibility of self-focusing of such discharges is demonstrated. The self-focusing is caused by a sharp slowdown in the speed of the radial ionization wave due to a change in the EEDF, a decrease in the average electron energy, electron mobility, and the rate of electron impact ionization in the crossed electric and magnetic fields as compared with the case of the discharge development without magnetic field. Simultaneously with the deceleration of the radial ionization wave, the ionization wave accelerates along the axis of the discharge gap due to a decrease in the radius of the streamer head and an increase in the electric field on it. Since the electric and magnetic fields are parallel to each other on the axis of symmetry, for the longitudinal wave there is no decrease in the average electron energy and ionization rate with an increase in the magnetic field value.

In a weakly ionized plasma, a transverse magnetic field slows down the heating of electrons in an external electric field. The effect of magnetic field on the electron properties is determined by the Hall parameter and turns out to be different for electrons belonging to different parts of their energy distribution function. In particular, in weakly ionized CO_2 plasma, the effect of magnetic field is most profound for electrons with energies in the 0.1–4 eV range and is less important for electrons with higher energies.

The self-focusing effect of a streamer discharge in an external longitudinal magnetic field is observed for both polarities of the discharge. At the same time, the self-focusing of the positive streamer is limited by a decrease in the photoionization efficiency as the streamer radius decreases to values less than the propagation distance of ionizing radiation in the gas. This limitation is absent for the negative streamer.

The estimates of the critical magnetic field obtained in this work lead to the conclusion that the effective interaction of the external magnetic field with the ionization wave occurs when the Hall parameter exceeds unity. For a qualitative assessment of this effect, it is proposed to consider the critical value of the reduced electron gyrofrequency $\omega_e/n \sim 10^{-13}$ rad \times m³/s (in CO_2), which may be somewhat different for other gases.

ACKNOWLEDGMENTS

This work was supported by DOE Grant No. DE-SC0021330, Texas A&M University/DOE–NETL, and DOE Grant No. DE-FE0026825.

APPENDIX: APPLICABILITY OF THE TWO-TERM APPROXIMATION FOR DESCRIBING ELECTRON DISTRIBUTION FUNCTION IN A STRONG MAGNETIC FIELD

The two-term approximation in the absence of magnetic field is reduced to the equation for the electron velocity distribution function (see, for instance, [44,47]),

$$f(\vec{u}) = f_0(u) + \cos\theta f_1(u), \quad (\text{A1})$$

where $f_0(u)$ and $f_1(u)$ are the isotropic and anisotropic parts of the distribution function, respectively, and θ is the angle between the vectors \vec{u} and the electric field strength \vec{E} . The two-term approximation is valid at small anisotropy when $f_1 \ll f_0$. The relation between the functions $f_0(u)$ and $f_1(u)$ is written as

$$f_1(u) = \frac{eE}{m_e v_m(u)} \frac{df_0(u)}{du}. \quad (\text{A2})$$

When an additional magnetic field \vec{B} is applied, Eq. (A1) is replaced by

$$f(\vec{u}) = f_0(u) + \frac{u_x}{u} f_{1x}(u) + \frac{u_y}{u} f_{1y}(u) + \frac{u_z}{u} f_{1z}(u), \quad (\text{A3})$$

where [47]

$$f_{1x}(u) = \frac{eE_{\perp} v_m(u)}{m_e(\omega_c^2 + v_m^2(u))} \frac{df_0(u)}{du}, \quad (\text{A4})$$

$$f_{1y}(u) = \frac{eE_{\perp} \omega_c}{m_e(\omega_c^2 + v_m^2(u))} \frac{df_0(u)}{du}, \quad (\text{A5})$$

and

$$f_{1z}(u) = \frac{eE_{\parallel}}{m_e v_m(u)} \frac{df_0(u)}{du}. \quad (\text{A6})$$

Here, \vec{B} is assumed to be directed along the z axis, $E_{\parallel} = E_z$ is the electric field component directed along \vec{B} , and $E_{\perp} = E_x$ is the electric field component directed normally to the vector \vec{B} . It follows from (A3)–(A5) that

$$\begin{aligned} f_1(B > 0) &= \sqrt{f_{1x}^2 + f_{1y}^2 + f_{1z}^2} \\ &= \frac{e}{m_e} \frac{df_0(u)}{du} \sqrt{\frac{E_{\perp}^2}{\omega_c^2 + v_m^2(u)} + \frac{E_{\parallel}^2}{v_m^2(u)}} \\ &< \frac{eE}{m_e v_m(u)} \frac{df_0(u)}{du}. \end{aligned} \quad (\text{A7})$$

We have from (A7) and (A2) that the anisotropy degree of the electron velocity distribution function does not increase with increasing magnetic field. Therefore, although a magnetic field leads to an additional anisotropy, the inequality $f_1 \ll f_0$ and the applicability of the two-term approximation are not violated when applying a strong magnetic field.

-
- [1] E. T. Curran and S. N. B. Murthy, Scramjet propulsion, in *Progress in Astronautics and Aeronautics* (American Institute of Aeronautics and Astronautics, Reston, VA, 2000), Vol. 189.
- [2] S. O. Macheret, M. N. Shneider, and R. B. Miles, Electron beam generated plasmas in hypersonic MHD channels, *AIAA J.* **39**, 1127 (2001).
- [3] S. O. Macheret, M. N. Shneider, and R. B. Miles, Magneto-hydrodynamic control of hypersonic flows and scramjet inlets using electron beam ionization, *AIAA J.* **40**, 74 (2002).
- [4] S. O. Macheret, M. N. Shneider, and R. B. Miles, MHD power extraction from cold hypersonic air flow with external ionizers, *J. Propul. Power* **18**, 424 (2002).
- [5] S. O. Macheret, M. N. Shneider, and R. B. Miles, Modeling of air plasma generation by electron beams and high-voltage pulses, in *31st Plasmadynamics and Lasers Conference* (American Institute of Aeronautics and Astronautics, Reston, VA, 2000).
- [6] S. O. Macheret, M. N. Shneider, and R. B. Miles, Modeling of air plasma generation by repetitive high-voltage nanosecond pulses, *IEEE Trans. Plasma Sci.* **30**, 1301 (2002).
- [7] E. Vallach, A. Zeevi, E. Greenfield, and S. Yatsiv, Transverse excitation pulsed laser in gas-dynamically cooled mixtures, *Appl. Phys. Lett.* **20**, 395 (1972).
- [8] J. H. Blom and R. K. Hanson, Double-discharge arrangement for cw electrical excitation of supersonic flows, *Appl. Phys. Lett.* **26**, 190 (1975).
- [9] T. G. Jones, S. R. Byron, A. L. Hoffman, B. B. O'Brian, and W. B. Lacuna, Electron-beam-stabilized cw electric discharge laser in supersonically cooled CO/N₂/Ar mixtures, in *7th Fluid and Plasmadynamics Conference* (American Institute of Aeronautics and Astronautics, Reston, VA, 1974).
- [10] B. M. Forestier, B. L. Fontaine, and P. Gross, Dynamics of supersonic flow excimer lasers, in *13th Fluid and Plasmadynamics Conference* (American Institute of Aeronautics and Astronautics, Reston, VA, 1980).
- [11] M. Uehara and H. Kanazawa, Experimental study on operation at room temperature of transverse flow carbon monoxide laser excited by radio frequency discharge, *Appl. Phys. Lett.* **65**, 22 (1994).
- [12] P. Palm, R. Meyer, E. Plonjes, W. Rich, and I. Adamovich, Nonequilibrium radio frequency discharge plasma effect on conical shock wave: $M = 2.5$ flow, *AIAA J.* **41**, 465 (2003).
- [13] N. A. Generalov, V. P. Zimakov, V. D. Kosynkin, Y. P. Raizer, and D. I. Roitenburg, Method for significantly increasing the stability limit of the discharge in fast-flow large-volume lasers, *Sov. Tech. Phys. Lett.* **1**(5), 201 (1975).
- [14] N. A. Generalov, V. P. Zimakov, V. D. Kosynkin, Y. P. Raizer, and D. I. Roitenburg, Steady externally sustained discharge with electrodeless pulsed ionization in a closed-loop laser. II. Theory of the capacitive discharge, *Sov. J. Plasma Phys.* **3**, 526 (1977).
- [15] N. A. Generalov, V. P. Zimakov, V. D. Kosynkin, Y. P. Raizer, and N. G. Solov'ev, Rapid-flow combined-action industrial CO₂ laser, *Sov. J. Quantum Electron.* **12**, 993 (1992).
- [16] R. J. Rosa, *Magneto-hydrodynamic Energy Conversion* (McGraw-Hill, New York, 1968).

- [17] R. C. Murray, S. H. Zaidi, M. R. Carraro, L. M. Vasilyak, S. O. Macheret, M. N. Shneider, and R. B. Miles, Magneto-hydrodynamic power generation using externally ionized, cold, supersonic air as working fluid, *AIAA J.* **44**, 119 (2006).
- [18] E. P. Velikhov, V. S. Golubev, and A. M. Dykhne, Physical phenomena in a low-temperature non-equilibrium plasma and in MHD generators with non-equilibrium conductivity, *At. Energy. Rev.* **14**, 325 (1976).
- [19] J. L. Kerrebrock, Nonequilibrium ionization due to electron heating: I. Theory, *AIAA J.* **2**, 1072 (1964).
- [20] E. M. Bazelyan and Yu. P. Raizer, *Spark Discharge* (CRC Press, Boca Raton, FL, 1998).
- [21] S. Nijdam, J. Teunissen, and U. Ebert, The physics of streamer discharge phenomena, *Plasma Sources Sci. Technol.* **29**, 103001 (2020).
- [22] K. Mitani and H. Kubo, Breakdown of argon at low pressure in a longitudinal magnetic field, *J. Phys. Soc. Jpn.* **15**, 678 (1960).
- [23] O. A. Omarov, A. A. Rukhadze, and A. S. Shikhaev, Plasma mechanism of gas breakdown in strong longitudinal magnetic fields, *Zh. Tekh. Fiz.* **52**, 255 (1982).
- [24] F. M. A. Al-Hareti, O. A. Omarov, N. O. Omarova, and P. Kh. Omarova, Influence of external magnetic fields on the energy characteristics of spark breakdown in high-pressure gases, *Probl. At. Sci. Technol., Ser.: Thermonucl. Fusion* **38**, 88 (2015), http://vant.iterru.ru/vant_2015_1/11.pdf.
- [25] M.-R. G. Kishov and N. A. Akopdzhanov, Investigation of gas breakdown in longitudinal and transverse magnetic fields, *Proc. High. Educ. Inst.: Radiophys.* **27**, 383 (1984).
- [26] M.-R. G. Kishov, Investigation of the process of formation of a cathode spot in a spark breakdown in helium in a strong longitudinal magnetic field, *Proc. High. Educ. Inst.: Radiophys.* **23**, 992 (1980).
- [27] A. T. Rakhimov and N. V. Suetin, Effect of longitudinal magnetic field on the development of near-electrode instability of a non-self-sustaining gas discharge, *Sov. Tech. Phys. Lett.* **10**, 121 (1984).
- [28] F. Manders, P. C. M. Christianen, and J. C. Maan, Propagation of a streamer discharge in a magnetic field, *J. Phys. D: Appl. Phys.* **41**, 234006 (2008).
- [29] M. Hara, J. Suehiro, and T. Wakiyama, Deflection of streamer channels in high magnetic field, *IEEE Trans. Electr. Insul.* **27**, 1179 (1992).
- [30] T. Han, L. Zhu, T. T. Ma, F. Y. Wang, B. X. Du, and Yu. Gao, Magnetic-field-dependent electrical tree under impulse-superimposed dc voltage at low temperature, *IEEE Trans. Appl. Supercond.* **29**, 8800205 (2019).
- [31] L. P. Babich, Ellipsoidal streamer model in longitudinal magnetic field, in *Proceedings of RFNC-VNIIEF* (RFNC-VNIIEF, Sarov, 2017) (in Russian), <http://book.sarov.ru/wp-content/uploads/2018/11/Works-RFNC-VNIIEF-v22-1.pdf>.
- [32] A. Yu. Starikovskiy and N. L. Aleksandrov, Gasdynamic diode: Streamer interaction with sharp density gradients, *Plasma Sources Sci. Technol.* **28**, 095022 (2019).
- [33] A. Yu. Starikovskiy and N. L. Aleksandrov, Blocking streamer development by plane gaseous layers of various densities, *Plasma Sources Sci. Technol.* **29**, 034002 (2020).
- [34] S. Pancheshnyi, M. Nudnova, and A. Starikovskiy, Development of a cathode-directed streamer discharge in air at different pressures: Experiment and comparison with direct numerical simulation, *Phys. Rev. E.* **71**, 016407 (2005).
- [35] S. V. Pancheshnyi and A. Yu. Starikovskiy, Stagnation dynamics of a cathode-directed streamer discharge in air, *Plasma Sources Sci. Technol.* **13**, B1 (2004).
- [36] S. V. Pancheshnyi and A. Yu. Starikovskiy, Two-dimensional numerical modeling of the cathode-directed streamer development in a long gap at high voltage, *J. Phys. D: Appl. Phys.* **36**, 2683 (2003).
- [37] S. V. Pancheshnyi, S. M. Starikovskaia, and A. Yu. Starikovskiy, Role of photoionization processes in propagation of cathode-directed streamer, *J. Phys. D: Appl. Phys.* **34**, 105 (2001).
- [38] S. V. Pancheshnyi, Photoionization produced by low-current discharges in O₂, air, N₂, and CO₂, *Plasma Sources Sci. Technol.* **24**, 015023 (2015).
- [39] C. Li, W. J. M. Brok, U. Ebert, and J. J. A. M. van der Mullen, Deviations from the local field approximation in negative streamer heads, *J. Appl. Phys.* **101**, 123305 (2007).
- [40] C. Li, U. Ebert, W. J. M. Brok, and W. Hundsdorfer, Spatial coupling of particle and fluid models for streamers: Where nonlocality matters, *J. Phys. D: Appl. Phys.* **41**, 032005 (2008).
- [41] C. Li, J. Teunissen, M. Nool, W. Hundsdorfer, and U. Ebert, A comparison of 3D particle, fluid, and hybrid simulations for negative streamers, *Plasma Sources Sci. Technol.* **21**, 055019 (2012).
- [42] A. H. Markosyan, S. Dujko, and U. Ebert, High-order fluid model for streamer discharges: II. Numerical solution and investigation of planar fronts, *J. Phys. D: Appl. Phys.* **46**, 475203 (2013).
- [43] A. H. Markosyan, J. Teunissen, S. Dujko, and U. Ebert, Comparing plasma fluid models of different order for 1D streamer ionization fronts, *Plasma Sources Sci. Technol.* **24**, 065002 (2015).
- [44] G. J. M. Hagelaar and L. C. Pitchford, Solving the Boltzmann equation to obtain electron transport coefficients and rate coefficients for fluid models, *Plasma Sources Sci. Technol.* **14**, 722 (2005).
- [45] BOLSIG+ Electron Boltzmann Equation Solver, <http://www.bolsig.laplace.univ-tlse.fr>.
- [46] SigloDataBase-LXCat-04, https://nl.lxcat.net/data/set_specB.php.
- [47] V. E. Golant, A. P. Zhilinsky, and I. F. Sakharov, *Fundamentals of Plasma Physics* (Wiley, New York, 1980).
- [48] A. Yu. Starikovskiy and N. L. Aleksandrov, How pulse polarity and photoionization control streamer discharge development in long air gaps, *Plasma Sources Sci. Technol.* **29**, 075004 (2020).
- [49] A. Yu. Starikovskiy, N. L. Aleksandrov, and M. N. Shneider, Simulation of decelerating streamers in inhomogeneous atmosphere with implications for runaway electron generation, *J. Appl. Phys.* **129**, 063301 (2021).
- [50] N. A. Dyatko, I. V. Kochetov, and A. P. Napartovich, Non-thermal plasma instabilities induced by deformation of the electron energy distribution function, *Plasma Sources Sci. Technol.* **23**, 043001 (2014).
- [51] N. L. Aleksandrov and I. V. Kochetov, Electron rate coefficients in gases under non-uniform field and electron density conditions, *J. Phys. D: Appl. Phys.* **29**, 1476 (1996).
- [52] N. L. Aleksandrov, N. A. Dyatko, and I. V. Kochetov, Rate of inelastic electron processes in a weakly ionized plasma in a nonstationary electric field, *Plasma Phys. Rep.* **21**, 763 (1995).